RIS-AIDED WIDEBAND DFRC WITH RECONFIGURABLE HOLOGRAPHIC SURFACE

Tong Wei, Linlong Wu, Kumar Vijay Mishra, M. R. Bhavani Shankar

⋆Interdisciplinary Centre for Security, Reliability and Trust (SnT), University of Luxembourg

ABSTRACT

Dual-function radar-communications (DFRC) systems generally employ reconfigurable intelligent surface (RIS) as a reflector in the wireless media to enable non-line-of-sight (NLoS) sensing and communications. Different from RIS, reconfigurable holographic surface (RHS) are the surfaces with an embedded feed. These surfaces are deployed at the transceiver thereby leading to a lightweight design and greater control of the *radiation amplitude*. In this paper, we propose a novel frequency-selective RIS-assisted wideband DFRC system that is also equipped with a RHS at the transceiver. Our goal is to jointly design the digital, holographic, and passive beamformers to maximize the radar signal-to-interference-plus-noise ratio (SINR) while ensuring the communication SINR among all users. The resulting nonconvex optimization problem involves maximin objective and difference of convex constraint. We develop an alternating maximization framework to decouple and iteratively solve these subproblems. Numerical experiments demonstrate that the proposed method achieves better radar performance than non-RHS, non-RIS, and randomly-configured RIS-aided DFRC systems.

***Index Terms*—** DFRC, frequency-selective beamforming, fractional optimization, RHS, RIS.

1. INTRODUCTION

A reconfigurable intelligent surface (RIS) consists of several passive or near-passive sub-wavelength metasurface elements [1]. In general, RIS is deployed as a reflector in the wireless media. By exploiting the non-line-of-sight (NLoS) paths, the RIS-aided sensing [2, 3] and communications [4, 5] systems extend their coverage [6, 7], suppress interference [5], and secure the information transfer [8]. Lately, these benefits are also shown to be useful [9, 10] for the emerging dual-function radar-communications (DFRC) [11], wherein sensing and communications jointly utilize the spectral and hardware resources.

Different from RIS, another metamaterial antenna called reconfigurable holographic surface (RHS) [12] has been proposed. The RHS is equipped with numerous metamaterial radiation elements that are integrated with the transceivers. The RHS provides a greater control of the *radiation amplitude* while also leading to compact and lightweight transceiver hardware [13, 14]. Initial RHS investigations were limited to wireless communications applications for flexible beam steering [15, 16]. Recently, it has been successfully deployed in the dual-function radar-communications (DFRC) system, which aligns the holographic beam towards the target and ensures the communication signal-to-interference-plus-noise ratio (SINR) [17]. However, even with the improved beam control, the RHS-aided systems yield poor performance in the absence of a stable line-of-sight (LoS) link thereby precipitating the need of also employing an RIS [18, 19].

Further, most of the prior research considers RIS-assisted wireless solutions for narrowband signaling that leads to frequency-independent passive beamformers. However, future DFRC systems are likely to operate at millimeter-wave or higher frequencies, where wideband processing is a necessity to harness the advantages of large bandwidths [11]. Narrowband RIS beamformers are not usable for such wideband systems, where the resulting beam-squint effect [20] could no longer be ignored.

To overcome the above-mentioned limitations, in this paper, we jointly exploit the advantages of both RIS and RHS in a wideband DFRC. We deploy the frequency-selective RIS [21] in the channel as a reflector while equipping the base-station (BS) with the RHS transceiver. We consider the problem of jointly designing the digital, holographic, and passive beamformers for the digital DFRC, RHS transceiver, and RIS, respectively. The objective is to maximize the radar SINR while also ensuring a minimum communications SINR over different users. The resulting optimization problem involves nonconvex quadratic constraint quadratic programming (QCQP) with coupled variables. We solve this challenging problem by first decoupling it into several subproblems which are solved via an alternating optimization (AO) algorithm.

Throughout this paper, we denote the vectors and matrices by boldface lowercase and uppercase letters, respectively. The notations $(\cdot)^T$, $(\cdot)^*$ and $(\cdot)^H$ denote transpose, conjugate, and Hermitian transpose, respectively; $\otimes$ is the Kronecker product; $\mathbf{I}_L$ is the $L \times L$ identity matrix; $\mathrm{diag}(\cdot)$ and $\mathrm{blkdiag}(\cdot)$ denote the diagonal and block diagonal matrix, respectively; $|\cdot|$ is the amplitude of complex-value; and $\|\cdot\|$ and $\|\cdot\|_F$ are the ℓ_2 and Frobenius norms, respectively.

2. SYSTEM MODEL

Consider an RIS-assisted wideband DFRC system (Fig.1), which employs orthogonal frequency-division multiplexing (OFDM) signaling with K subcarriers. The coverage area comprises of a radar target, Q clutter patches, and U mobile users. The BS is equipped with an RHS fed by N_{RF} radio-frequency (RF) chains. The antenna elements at BS (RIS, user) along the x- and y-axes are N_x^B (N_x^R, N_x^U) and N_y^B (N_y^R, N_y^U), respectively. The frequency-dependent (wideband) steering vectors of BS, RIS, and user are, respectively,

$$\mathbf{a}_B(f_k,\theta,\psi) = [1,\cdots,e^{-j\frac{2\pi}{\lambda_k}((N_x^B-1)\mu_x^B+(N_y^B-1)\mu_y^B)}]^T, \quad (1)$$

$$\mathbf{a}_R(f_k,\theta,\psi) = [1,\cdots,e^{-j\frac{2\pi}{\lambda_k}((N_x^R-1)\mu_x^R+(N_y^R-1)\mu_y^R)}]^T, \quad (2)$$

$$\mathbf{a}_U(f_k,\theta,\psi) = [1,\cdots,e^{-j\frac{2\pi}{\lambda_k}((N_x^U-1)\mu_x^U+(N_y^U-1)\mu_y^U)}]^T, \quad (3)$$

where $\theta \in [0, 2\pi]$ and $\psi \in [0, \frac{\pi}{2}]$ are azimuth and elevation angles, respectively, λ_k is the wavelength of k-th subcarrier, f_k denotes the central and k-th subcarrier offset frequency, $\mu_x = d_x \cos\theta\cos\psi$, $\mu_y = d_y \sin\theta\cos\psi$ is the directional cosines, and d_x (d_y) is the inter-element spacing along the x- (y-) direction.

Assume θ_{BR}, θ_{Bu}, and θ_{Bt}, θ_{Bq} (ψ_{BR}, ψ_{Bu}, ψ_{Bt}, and ψ_{Bq}) are the azimuth (elevation) angles from dual-function base station (DFBS) to the RIS, u-th user, target, and q-th clutter, respectively. Similarly, denote the azimuth (elevation) angles from the RIS to DFBS, u-th user, target, and q-th clutter by θ_{RB}, θ_{Ru}, θ_{Rt}, and θ_{Rq} (ψ_{RB}, ψ_{Ru}, ψ_{Rt}, and ψ_{Rq}), respectively.

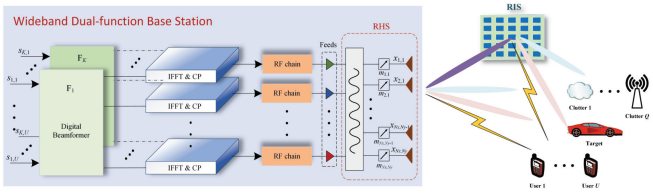

Fig. 1. Illustration of RIS-aided wideband DFRC with RHS.

Wideband RHS Transmitter: The transmit symbol vector at the k-th subcarrier is $\mathbf{s}_k = [s_{k,1}, \cdots, s_{k,U}]^T \in \mathbb{C}^{U\times 1}$. The frequency-domain signal at k-th subcarrier after the digital beamforming is

$$\widetilde{\mathbf{x}}_T[f_k] = \mathbf{F}_k\mathbf{s}_k \in \mathbb{C}^{N_{RF}\times 1}, k = 1, \cdots, K, \tag{4}$$

where $\mathbf{F}_k$ denotes the frequency-dependent beamformer to mitigate the beam-squint [22]. Aplying N_{RF} K-point inverse fast Fourier transform to (4) yields

$$\mathbf{x}_T(t) = \sum\nolimits_{k=1}^{K} \mathbf{F}_k\mathbf{s}_k e^{\mathrm{j}2\pi f_k t} \in \mathbb{C}^{N_{RF}\times 1}, t \in (0, T_s], \tag{5}$$

where T_s denotes the OFDM duration (excluding the cyclic prefix (CP)). The RHS has N_{RF} feeds and $N_x^B \times N_y^B$ discrete elements[1]. At the k-th subcarrier, its electromagnetic response is [15]

$$\mathbf{V}[f_k] = \mathbf{M}\mathbf{V}_k \in \mathbb{C}^{N_x^B N_y^B \times N_{RF}}, \tag{6}$$

where $\mathbf{V}_k(p,q) = e^{-2\pi\gamma D_{p,q}/\lambda_k}$, the matrix $\mathbf{M} = \mathrm{diag}\left[m_{1,1}, \cdots, m_{1,N_y^B}, \cdots, m_{N_x^B,1}, \cdots, m_{N_x^B,N_y^B}\right]$, $0 \le m_{x,y} \le 1$ is the amplitude-control beamformer of (x,y)-th RHS element, $D_{p,q}$ denotes the distance between the p-th RHS element and q-th feed, $p = 1, \cdots, N_x^B N_y^B, q = 1, \cdots, N_{RF}$, and γ is the refractive index of the RHS material. Hence, if the structure of holographic surface is fixed, the matrix $\mathbf{V}_k, k = 1, \cdots, K$ is known. Hence, after the digital and holographic beamformer and upconversion, the transmitted signal of RHS excluding CP becomes

$$\mathbf{x}(t) = \mathbf{M}\sum\nolimits_{k=1}^{K} \mathbf{V}_k\mathbf{F}_k\mathbf{s}_k e^{\mathrm{j}2\pi(f_k+f_c)t}. \tag{7}$$

Received signal at the u-th communications user: Subsequent to baseband conversion, CP removal and K-point FFT, the received signal of u-th user on the k-th subcarrier is

$$\begin{aligned}\mathbf{y}_{C_u}[f_k] =& \mathbf{H}_{C_u,k}\mathbf{M}\mathbf{V}_k\mathbf{F}_k\mathbf{s}_k + \mathbf{n}_{C_u}[f_k] \\ =& (\mathbf{H}_{C_u,k}^{\mathrm{dir}} + \mathbf{H}_{C_u,k}^{\mathrm{RIS}}\mathbf{\Phi}_k\mathbf{G}_k)\mathbf{M}\mathbf{V}_k\mathbf{F}_k\mathbf{s}_k + \mathbf{n}_{C_u}[f_k],\end{aligned} \tag{8}$$

where $\mathbf{H}_{C_u,k}$ denotes the composite channel between BS and u-th user, $\mathbf{\Phi}_k$ denotes the frequency-dependent phase-shift matrix [21], $\mathbf{n}_{C_u}[f_k]$ denotes the receiver front end noise at the k-th subcarrier with zero mean and covariance $\sigma_r^2\mathbf{I}$, and the wideband channel is

$$\mathbf{G}_k = g_{BR,k}\mathbf{a}_R(f_k, \theta_{RB}, \psi_{RB})\mathbf{a}_B^T(f_k, \theta_{BR}, \psi_{BR}), \tag{9}$$

$$\begin{aligned}\mathbf{H}_{C_u,k}^{\mathrm{dir}} =& \sqrt{\frac{\Upsilon}{1+\Upsilon}} g_{Bu,k}\mathbf{a}_u(f_k, \theta_{uB}, \psi_{uB})\mathbf{a}_B^T(f_k, \theta_{Bu}, \psi_{Bu}) \\ &+ \sqrt{\frac{1}{1+\Upsilon}} \sum_{l_d=1}^{L_d} g_{l_d,k}\mathbf{a}_u(f_k, \hat{\theta}_{l_d}, \hat{\psi}_{l_d})\mathbf{a}_B^T(f_k, \theta_{l_d}, \psi_{l_d}),\end{aligned} \tag{10}$$

$$\begin{aligned}\mathbf{H}_{C_u,k}^{\mathrm{RIS}} =& \sqrt{\frac{\Upsilon}{1+\Upsilon}} g_{Ru,k}\mathbf{a}_u(f_k, \theta_{uR}, \psi_{uR})\mathbf{a}_R^T(f_k, \theta_{Ru}, \psi_{Ru}) \\ &+ \sqrt{\frac{1}{1+\Upsilon}} \sum_{l_r=1}^{L_r} g_{l_r,k}\mathbf{a}_u(f_k, \hat{\theta}_{l_r}, \hat{\psi}_{l_r})\mathbf{a}_B^T(f_k, \theta_{l_r}, \psi_{l_r}),\end{aligned} \tag{11}$$

where $g_{*,k} = \mathcal{P}_k(\frac{c}{4\pi r f_k})^\epsilon$ is the free-space path loss, r is the distance of the corresponding path and $\mathcal{P}_k$ is the maximum power assigned to the k-th subcarrier, Υ denote the Rician factor, $\mathbf{H}_{C_u,k}^{\mathrm{dir}}$ is the direct BS-user, $\mathbf{H}_{C_u,k}^{\mathrm{RIS}}$ is the RIS-user channel, and $\mathbf{G}_k$ is the DFBS-RIS channel in which only the LoS component is considered. The aforementioned channels are estimated *a priori* [23, 24].

To estimate the symbol of u-th user, the digital combiner $\mathbf{w}_{k,u}$ is utilized to filter the received signal as

$$\begin{aligned}\tilde{s}_{k,u} =& \mathbf{w}_{k,u}^H\mathbf{y}_{C_u}[f_k] \\ =& \mathbf{w}_{k,u}^H\mathbf{H}_{C_u,k}\mathbf{M}\mathbf{V}_k\mathbf{f}_{k,u}s_{k,u} \\ &+ \sum\nolimits_{i\neq u}^{U} \mathbf{w}_{k,u}^H\mathbf{H}_{C_u,k}\mathbf{M}\mathbf{V}_k\mathbf{f}_{k,i}s_{k,i} + \mathbf{w}_{k,u}^H\mathbf{n}_{C_u}[f_k].\end{aligned} \tag{12}$$

Based on (12), we can define the average SINR of u-th user as

$$\mathrm{SINR}_{C_u} = \frac{\sum_{k=1}^{K}\|\mathbf{w}_{k,u}^H\mathbf{H}_{C_u,k}\mathbf{M}\mathbf{V}_k\mathbf{F}_k\mathbf{\Lambda}_u\|^2}{\sum_{k=1}^{K}(\|\mathbf{w}_{k,u}^H\mathbf{H}_{C_u,k}\mathbf{M}\mathbf{V}_k\mathbf{F}_k\widetilde{\mathbf{\Lambda}}_u\|^2 + \sigma_e^2\mathbf{w}_{k,u}^H\mathbf{w}_{k,u})}, \tag{13}$$

where $\mathbf{\Lambda}_u$ denotes the selection matrix with u-th diagonal element is one and the others are zero and $\widetilde{\mathbf{\Lambda}}_u = \mathbf{I}_U - \mathbf{\Lambda}_u$.

Received signal from the radar target: Similarly, for the radar receiver, the echo signal on the k-th subcarrier

$$\mathbf{y}_R[f_k] = (\mathbf{H}_{R_t,k} + \sum\nolimits_{q=1}^{Q}\mathbf{H}_{R_q,k})\mathbf{M}\mathbf{V}_k\mathbf{F}_k\mathbf{s}_k + \mathbf{n}_R[f_k], \tag{14}$$

where the composite channels across DFBS-target-receiver and DFBS-clutter q-receiver are, respectively,

$$\mathbf{H}_{R_t,k} = (\mathbf{h}_{R_t,k} + \mathbf{G}_k^T\mathbf{\Phi}_k\mathbf{b}_{R_t,k})(\mathbf{h}_{R_t,k}^T + \mathbf{b}_{R_t,k}^T\mathbf{\Phi}_k\mathbf{G}_k), \tag{15}$$

$$\mathbf{H}_{R_q,k} = (\mathbf{h}_{R_q,k} + \mathbf{G}_k^T\mathbf{\Phi}_k\mathbf{b}_{R_q,k})(\mathbf{h}_{R_q,k}^T + \mathbf{b}_{R_q,k}^T\mathbf{\Phi}_k\mathbf{G}_k). \tag{16}$$

where $\mathbf{h}_{R_t,k} = g_{Bt,k}\mathbf{a}_B(f_k, \theta_{Bt}, \psi_{Bt})$ denotes the channel from target to DFBS and $\mathbf{b}_{R_t,k} = g_{Rt,k}\mathbf{a}_R(f_k, \theta_{Rt}, \psi_{Rt})$ denotes the channel from target to RIS. Based on (14), define the radar SINR as

$$\mathrm{SINR}_{R_t} = \frac{\sum_{k=1}^{K}\|\mathbf{w}_{k,t}^H\mathbf{H}_{R_t,k}\mathbf{M}\mathbf{V}_k\mathbf{F}_k\|_2^2}{\sum_{k=1}^{K}\sum_{q=1}^{Q}\|\mathbf{w}_{k,t}^H\mathbf{H}_{R_q,k}\mathbf{M}\mathbf{V}_k\mathbf{F}_k\|_2^2 + \sigma_r^2\mathbf{w}_{k,t}^H\mathbf{w}_{k,t}}, \tag{17}$$

where $\mathbf{w}_{k,t}$ denotes the radar receive filter at the k-subcarrier. In order to enhance the target detection performance, the corresponding SINR should be maximized, and the impact of echo signal from clutter needs to be simultaneously minimized.

[1]Note that the number of feed should be great or equal to the number of active data symbols in order to guarantee the decode performance but less than the number of RHS element to reduce the hardware cost.

Beamformers design: Our goal in a radar-centric DFRC is to maximize the radar SINR while guaranteeing the communication SINR over all users. We formulate this optimization problem as

$$\begin{aligned}\underset{\mathbf{w}_{k,t},\mathbf{w}_{k,u},\mathbf{F}_k,\mathbf{\Phi}_k,\mathbf{M}}{\text{maximize}} \quad & \text{SINR}_{R_t} && \text{(18a)}\\ \text{subject to} \quad & \text{SINR}_{C_u} \geq \eta, \forall u, && \text{(18b)}\\ & \|\mathbf{M}\mathbf{V}_k\mathbf{F}_k\|_F^2 \leq \mathcal{P}_k, \forall k, && \text{(18c)}\\ & 0 \leq m_{n_x^B,n_y^B} \leq 1, \forall i, |\mathbf{\Phi}_k| = 1, \forall k, && \text{(18d)}\end{aligned}$$

where $m_{n_x,n_y}=0$ denotes the (n_x, n_y)-th RHS element is disabled and $m_{n_x,n_y}=1$ denotes the (n_x, n_y)-th RHS element is fully utilized, and η denotes the threshold of communication user. Note that the above optimization problem involves the maximin objective function, difference of convex (DC). and unimodular constraints. It is highly nonconvex and thus difficult to directly solve.

3. ALTERNATING OPTIMIZATION

We first decouple the nonconvex QCQP into four subproblems of designing the receive filter along with digital, holographic, and passive beamformers. Then, we resort to AO to solve these problems.

Update of receive filter $\mathbf{w}_{k,t}$: We first define the communication filter $\mathbf{w}_u = [\mathbf{w}_{1,u}^T, \cdots, \mathbf{w}_{K,u}^T]^T$ and radar filter $\mathbf{w}_t = [\mathbf{w}_{1,t}^T, \cdots, \mathbf{w}_{K,t}^T]^T$ for all subcarriers. Then, for fixed $\mathbf{\Phi}_k, \mathbf{F}_k$ and $\mathbf{M}$, the subproblem with respect to $\mathbf{w}_{k,t}$ and $\mathbf{w}_{k,u}$ is

$$\mathcal{P}_1 \begin{cases} \underset{\mathbf{w}_t,\mathbf{w}_u}{\text{maximize}} & \dfrac{\mathbf{w}_t^H \mathbf{\Sigma}_t^{\mathcal{P}_1} \mathbf{w}_t}{\mathbf{w}_t^H \widetilde{\mathbf{\Sigma}}_t^{\mathcal{P}_1} \mathbf{w}_t + \sigma_r^2 \mathbf{w}_t^H \mathbf{w}_t}, \\ \text{subject to} & \dfrac{\mathbf{w}_u^H \mathbf{\Sigma}_u^{\mathcal{P}_1} \mathbf{w}_u}{\mathbf{w}_u^H \widetilde{\mathbf{\Sigma}}_u^{\mathcal{P}_1} \mathbf{w}_u + \sigma_c^2 \mathbf{w}_u^H \mathbf{w}_u} \geq \eta, \forall u \end{cases} \tag{19}$$

where the block diagonal matrix w.r.t $\mathcal{P}_1$ is given by

$$\begin{aligned}\mathbf{\Sigma}_t^{\mathcal{P}_1} &= \text{blkdiag}[\mathbf{\Sigma}_{1,t}^{\mathcal{P}_1}, \cdots, \mathbf{\Sigma}_{K,t}^{\mathcal{P}_1}], && \text{(20a)}\\ \widetilde{\mathbf{\Sigma}}_t^{\mathcal{P}_1} &= \text{blkdiag}[\widetilde{\mathbf{\Sigma}}_{1,t}^{\mathcal{P}_1}, \cdots, \widetilde{\mathbf{\Sigma}}_{K,t}^{\mathcal{P}_1}], && \text{(20b)}\\ \mathbf{\Sigma}_u^{\mathcal{P}_1} &= \text{blkdiag}[\mathbf{\Sigma}_{1,u}^{\mathcal{P}_1}, \cdots, \mathbf{\Sigma}_{K,u}^{\mathcal{P}_1}], u = 1, \cdots, U, && \text{(20c)}\\ \widetilde{\mathbf{\Sigma}}_u^{\mathcal{P}_1} &= \text{blkdiag}[\widetilde{\mathbf{\Sigma}}_{1,u}^{\mathcal{P}_1}, \cdots, \widetilde{\mathbf{\Sigma}}_{K,u}^{\mathcal{P}_1}], u = 1, \cdots, U. && \text{(20d)}\end{aligned}$$

and

$$\begin{aligned}\mathbf{\Sigma}_{k,u}^{\mathcal{P}_1} &= \mathbf{H}_{C_u,k}\mathbf{M}\mathbf{V}_k\mathbf{F}_k\mathbf{\Lambda}\mathbf{F}_k^H\mathbf{V}_k^H\mathbf{M}^H\mathbf{H}_{C_u,k}^H, && \text{(21a)}\\ \widetilde{\mathbf{\Sigma}}_{k,u}^{\mathcal{P}_1} &= \mathbf{H}_{C_u,k}\mathbf{M}\mathbf{V}_k\mathbf{F}_k\widetilde{\mathbf{\Lambda}}\mathbf{F}_k^H\mathbf{V}_k^H\mathbf{M}^H\mathbf{H}_{C_u,k}^H, && \text{(21b)}\\ \mathbf{\Sigma}_{k,t}^{\mathcal{P}_1} &= \mathbf{H}_{R_t,k}\mathbf{M}\mathbf{V}_k\mathbf{F}_k\mathbf{F}_k^H\mathbf{V}_k^H\mathbf{M}\mathbf{H}_{R_t,k}^H, && \text{(21c)}\\ \widetilde{\mathbf{\Sigma}}_{k,t}^{\mathcal{P}_1} &= \sum\nolimits_{q=1}^{Q}\mathbf{H}_{R_q,k}\mathbf{M}\mathbf{V}_k\mathbf{F}_k\mathbf{F}_k^H\mathbf{V}_k^H\mathbf{M}\mathbf{H}_{R_q,k}^H. && \text{(21d)}\end{aligned}$$

To simplify the design process, we fix the digital combiner of user as all one vector and the related optimization problem will be discussed in the full version of this work. Then, $\mathcal{P}_1$ can be tackled by solving

$$\underset{\mathbf{w}_t}{\text{maximize}} \quad \frac{\mathbf{w}_t^H \mathbf{\Sigma}_t^{\mathcal{P}_1} \mathbf{w}_t}{\mathbf{w}_t^H \widetilde{\mathbf{\Sigma}}_t^{\mathcal{P}_1} \mathbf{w}_t + \sigma_r^2 \mathbf{w}_t^H \mathbf{w}_t}. \tag{22}$$

Notice that Problem (22) is composed of a set of generalized Rayleigh quotient programming in which the closed-form solution can be given by

$$\mathbf{w}_t^* = \rho((\widetilde{\mathbf{\Sigma}}_t^{\mathcal{P}_1} + \sigma_r^2 \mathbf{I}_{N^B K})^{-1} \mathbf{\Sigma}_t^{\mathcal{P}_1}), t = 1, \cdots, T, \tag{23}$$

where $\rho(\cdot)$ denotes the operation of principal eigenvector.

Update of digital beamforming $\mathbf{F}_k$:

$$\mathcal{P}_2 \begin{cases} \underset{\mathbf{f}}{\text{maximize}} & \dfrac{\mathbf{f}^H \mathbf{\Sigma}_t^{\mathcal{P}_2} \mathbf{f}}{\mathbf{f}^H \widetilde{\mathbf{\Sigma}}_t^{\mathcal{P}_2} \mathbf{f} + \sigma_r^2 \mathbf{w}_t^H \mathbf{w}_t} \\ \text{subject to} & \|\mathbf{S}_k \mathbf{\Xi} \mathbf{f}\|_2^2 \leq \mathcal{P}_k, \forall k, \\ & \dfrac{\mathbf{f}^H \mathbf{\Sigma}_u^{\mathcal{P}_2} \mathbf{f}}{\mathbf{f}^H \widetilde{\mathbf{\Sigma}}_u^{\mathcal{P}_2} \mathbf{f} + \sigma_c^2 \mathbf{w}_u^H \mathbf{w}_u} \geq \eta, \forall u, \end{cases} \tag{24}$$

where $\mathbf{f} = [\text{vec}(\mathbf{F}_1)^T, \cdots, \text{vec}(\mathbf{F}_K)^T]^T$, $\mathbf{S}_k$ denotes the selection matrix to extract k-th interval of vector, $\mathbf{\Xi} = \text{blkdiag}[(\mathbf{I}_U \otimes \mathbf{M}\mathbf{V}_1), \cdots, (\mathbf{I}_U \otimes \mathbf{M}\mathbf{V}_K)]$, and the block diagonal matrices $\mathbf{\Sigma}_t^{\mathcal{P}_2}$, $\widetilde{\mathbf{\Sigma}}_t^{\mathcal{P}_2}$, $\mathbf{\Sigma}_u^{\mathcal{P}_2}$ and $\widetilde{\mathbf{\Sigma}}_u^{\mathcal{P}_2}$ are similarly defined as (20) and we omit it herein due to the space limitation.

Note that $\mathcal{P}_2$ is highly nonconvex due to the fractional quadratic objective function and second constraint. Hence, we simplify it via the first-order Taylor approximation as

$$\mathcal{P}_{2.1} \begin{cases} \underset{\mathbf{f}}{\text{maximize}} & \dfrac{2\Re(\mathbf{f}^{(l)H} \mathbf{\Sigma}_t^{\mathcal{P}_2} \mathbf{f}) - \mathbf{f}^{(l)H} \mathbf{\Sigma}_t^{\mathcal{P}_2} \mathbf{f}^{(l)}}{\mathbf{f}^H \widetilde{\mathbf{\Sigma}}_t^{\mathcal{P}_2} \mathbf{f} + \sigma_r^2 \mathbf{w}_t^H \mathbf{w}_t} \\ \text{subject to} & \|\mathbf{S}_k \mathbf{\Xi} \mathbf{f}\|_2^2 \leq \mathcal{P}_k, \forall k, \\ & \dfrac{2\Re(\mathbf{f}^{(l)H} \mathbf{\Sigma}_u^{\mathcal{P}_2} \mathbf{f}) - \mathbf{f}^{(l)H} \mathbf{\Sigma}_u^{\mathcal{P}_2} \mathbf{f}^{(l)}}{\mathbf{f}^H \widetilde{\mathbf{\Sigma}}_u^{\mathcal{P}_2} \mathbf{f} + \sigma_c^2 \mathbf{w}_u^H \mathbf{w}_u} \geq \eta, \forall u, \end{cases} \tag{25}$$

This is a standard fractional maximization problem that can be solved using Dinkelbach-based method [25, 26].

Update of holographic beamformer $\mathbf{M}$:

$$\mathcal{P}_3 \begin{cases} \underset{\mathbf{0} \preceq \mathbf{m} \preceq \mathbf{1}}{\text{maximize}} & \dfrac{\mathbf{m}^T \Re(\mathbf{\Sigma}_t^{\mathcal{P}_3}) \mathbf{m}}{\mathbf{m}^T \Re(\widetilde{\mathbf{\Sigma}}_t^{\mathcal{P}_3}) \mathbf{m} + \sigma_r^2 \mathbf{w}_t^H \mathbf{w}_t} \\ \text{subject to} & \|\text{diag}(\mathbf{m}) \mathbf{V}_k \mathbf{F}_k\|_F^2 \leq \mathcal{P}_k, \forall k, \\ & \dfrac{\mathbf{m}^T \Re(\mathbf{\Sigma}_u^{\mathcal{P}_3}) \mathbf{m}}{\mathbf{m}^T \Re(\widetilde{\mathbf{\Sigma}}_u^{\mathcal{P}_3}) \mathbf{m} + \sigma_c^2 \mathbf{w}_u^H \mathbf{w}_u} \geq \eta, \forall u, \end{cases} \tag{26}$$

where $\mathbf{m} = \mathbf{M}^T \mathbf{1}_{N_x N_y}$ and the matrices $\mathbf{\Sigma}_t^{\mathcal{P}_3}$, $\widetilde{\mathbf{\Sigma}}_t^{\mathcal{P}_3}$, $\mathbf{\Sigma}_u^{\mathcal{P}_3}$ and $\widetilde{\mathbf{\Sigma}}_u^{\mathcal{P}_3}$ are similarly defined as (20) which are omitted it herein. Similar to $\mathcal{P}_2$, reformulate $\mathcal{P}_3$ as

$$\mathcal{P}_{3.1} \begin{cases} \underset{\mathbf{0} \preceq \mathbf{m} \preceq \mathbf{1}}{\text{maximize}} & \dfrac{2\mathbf{m}^{(l)T} \Re(\mathbf{\Sigma}_t^{\mathcal{P}_3}) \mathbf{m} - \mathbf{m}^{(l)T} \Re(\mathbf{\Sigma}_t^{\mathcal{P}_3}) \mathbf{m}^{(l)}}{\mathbf{m}^T \Re(\widetilde{\mathbf{\Sigma}}_t^{\mathcal{P}_3}) \mathbf{m} + \sigma_r^2 \mathbf{w}_t^H \mathbf{w}_t} \\ \text{subject to} & \|\text{diag}(\mathbf{m}) \mathbf{V}_k \mathbf{F}_k\|_F^2 \leq \mathcal{P}_k, \forall k, \\ & \dfrac{2\mathbf{m}^{(l)T} \Re(\mathbf{\Sigma}_u^{\mathcal{P}_3}) \mathbf{m} - \mathbf{m}^{(l)T} \Re(\mathbf{\Sigma}_u^{\mathcal{P}_3}) \mathbf{m}^{(l)}}{\mathbf{m}^T \Re(\widetilde{\mathbf{\Sigma}}_u^{\mathcal{P}_3}) \mathbf{m} + \sigma_c^2 \mathbf{w}_u^H \mathbf{w}_u} \geq \eta, \forall u. \end{cases} \tag{27}$$

This subproblem is similar to the previous $\mathcal{P}_{2.1}$ and Dinkelbach-based method is applicable here.

Update of passive beamformer $\mathbf{\Phi}_k$: With the fixed $\mathbf{w}_{k,t}$, $\mathbf{w}_{k,u}$, $\mathbf{F}_k$, $\mathbf{M}$, the subproblem w.r.t phase-shift design is

$$\mathcal{P}_4 \begin{cases} \underset{\boldsymbol{\phi},\boldsymbol{\varphi}}{\text{maximize}} & \text{SINR}_{R_t} \\ \text{subject to} & |\boldsymbol{\phi}| = 1, |\boldsymbol{\varphi}| = 1, \boldsymbol{\phi} = \boldsymbol{\varphi}, \\ & \dfrac{\boldsymbol{\phi}^T \mathbf{\Sigma}_u^{\mathcal{P}_4} \boldsymbol{\phi}^* + 2\Re(\boldsymbol{\phi}^T \mathbf{d}_u^{\mathcal{P}_4}) + d_u^{\mathcal{P}_4}}{\boldsymbol{\phi}^T \widetilde{\mathbf{\Sigma}}_u^{\mathcal{P}_4} \boldsymbol{\phi}^* + 2\Re(\boldsymbol{\phi}^T \widetilde{\mathbf{d}}_u^{\mathcal{P}_4}) + \tilde{d}_u^{\mathcal{P}_4}} \geq \eta, \forall u, \end{cases} \tag{28}$$

where $d_u^{\mathcal{P}_4} = \sum_{k=1}^K d_{k,u}^{\mathcal{P}_4}$, $\mathbf{d}_u^{\mathcal{P}_4} = [\mathbf{d}_{1,u}^{\mathcal{P}_4}; \cdots; \mathbf{d}_{K,u}^{\mathcal{P}_4}]$, $\tilde{d}_u^{\mathcal{P}_4} = \sum_{k=1}^K \tilde{d}_{k,u}^{\mathcal{P}_4} + \sigma_c^2 \mathbf{w}_u^H \mathbf{w}_u$, $\widetilde{\mathbf{d}}_u^{\mathcal{P}_4} = [\widetilde{\mathbf{d}}_{1,u}^{\mathcal{P}_4}; \cdots; \widetilde{\mathbf{d}}_{K,u}^{\mathcal{P}_4}]$, $\mathbf{\Sigma}_u^{\mathcal{P}_4}$ and $\widetilde{\mathbf{\Sigma}}_u^{\mathcal{P}_4}$

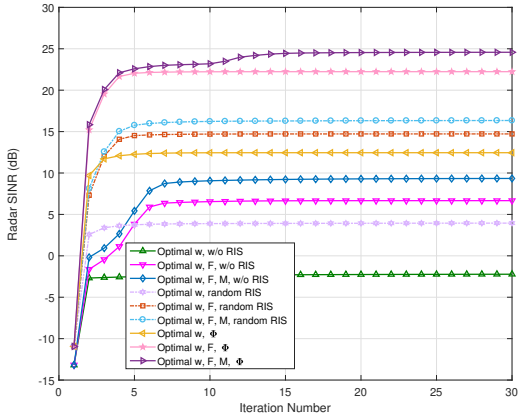

Fig. 2. Radar SINR versus number of iterations.

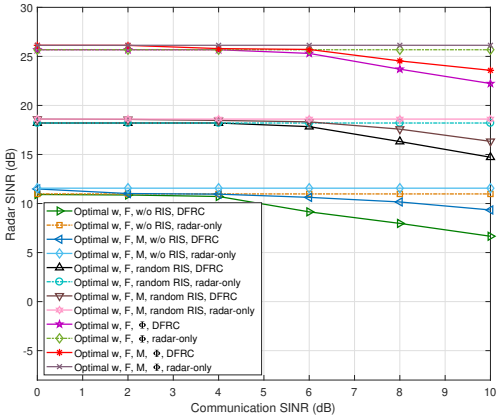

Fig. 3. Radar SINR versus Communication SINR.

are similarly defined as (20) and hence we omit it here due to limited space. For the unit-sphere programming, it is solved by Riemannian steepest decent (RSD) algorithm [27]. The, $\mathcal{P}_4$ is reformulated as

$$\mathcal{P}_{4.1}\begin{cases}\underset{\boldsymbol{\phi},\boldsymbol{\varphi}}{\text{maximize}}\ \dfrac{f_t(\boldsymbol{\phi},\boldsymbol{\varphi})}{g_t(\boldsymbol{\phi},\boldsymbol{\varphi})}\\ \text{subject to } |\boldsymbol{\phi}|=1, |\boldsymbol{\varphi}|=1, \boldsymbol{\phi}-\boldsymbol{\varphi}=\mathbf{0},\\ \qquad\qquad \dfrac{\boldsymbol{\phi}^T\boldsymbol{\Sigma}_u^{\mathcal{P}_4}\boldsymbol{\phi}^*+2\Re(\boldsymbol{\phi}^T\mathbf{d}_u^{\mathcal{P}_4})+d_u^{\mathcal{P}_4}}{\boldsymbol{\phi}^T\widetilde{\boldsymbol{\Sigma}}_u^{\mathcal{P}_4}\boldsymbol{\phi}^*+2\Re(\boldsymbol{\phi}^T\widetilde{\mathbf{d}}_u^{\mathcal{P}_4})+\tilde{d}_u^{\mathcal{P}_4}}\geq\eta,\forall u,\end{cases} \tag{29}$$

where

$$f_t(\boldsymbol{\phi},\boldsymbol{\varphi})=\boldsymbol{\phi}^T\boldsymbol{\Sigma}_t^{\mathcal{P}_4}(\boldsymbol{\varphi})\boldsymbol{\phi}^*+2\Re(\boldsymbol{\phi}^T\mathbf{d}_t^{\mathcal{P}_4}(\boldsymbol{\varphi}))+d_t^{\mathcal{P}_4}(\boldsymbol{\varphi}) \tag{30a}$$

$$=\boldsymbol{\varphi}^T\boldsymbol{\Sigma}_t^{\mathcal{P}_4}(\boldsymbol{\phi})\boldsymbol{\varphi}^*+2\Re(\boldsymbol{\varphi}^T\mathbf{d}_t^{\mathcal{P}_4}(\boldsymbol{\phi}))+d_t^{\mathcal{P}_4}(\boldsymbol{\phi}), \tag{30b}$$

$$g_t(\boldsymbol{\phi},\boldsymbol{\varphi})=\boldsymbol{\phi}^T\widetilde{\boldsymbol{\Sigma}}_t^{\mathcal{P}_4}(\boldsymbol{\varphi})\boldsymbol{\phi}^*+2\Re(\boldsymbol{\phi}^T\widetilde{\mathbf{d}}_t^{\mathcal{P}_4}(\boldsymbol{\varphi}))+\tilde{d}_t^{\mathcal{P}_4}(\boldsymbol{\varphi}) \tag{30c}$$

$$=\boldsymbol{\varphi}^T\widetilde{\boldsymbol{\Sigma}}_t^{\mathcal{P}_4}(\boldsymbol{\phi})\boldsymbol{\varphi}^*+2\Re(\boldsymbol{\varphi}^T\widetilde{\mathbf{d}}_t^{\mathcal{P}_4}(\boldsymbol{\phi}))+\tilde{d}_t^{\mathcal{P}_4}(\boldsymbol{\phi}). \tag{30d}$$

Rewrite the problem $\mathcal{P}_{4.1}$ as

$$\mathcal{P}_{4.2}\begin{cases}\underset{\boldsymbol{\phi},\boldsymbol{\varphi}}{\text{maximize}}\ f_t(\boldsymbol{\phi},\boldsymbol{\varphi})-\lambda_{\boldsymbol{\phi}}g_t(\boldsymbol{\phi},\boldsymbol{\varphi})\\ \text{subject to } |\boldsymbol{\phi}|=1, |\boldsymbol{\varphi}|=1, \boldsymbol{\phi}-\boldsymbol{\varphi}=\mathbf{0},\\ \qquad\qquad \dfrac{\boldsymbol{\phi}^T\boldsymbol{\Sigma}_u^{\mathcal{P}_4}\boldsymbol{\phi}^*+2\Re(\boldsymbol{\phi}^T\mathbf{d}_u^{\mathcal{P}_4})+d_u^{\mathcal{P}_4}}{\boldsymbol{\phi}^T\widetilde{\boldsymbol{\Sigma}}_u^{\mathcal{P}_4}\boldsymbol{\phi}^*+2\Re(\boldsymbol{\phi}^T\widetilde{\mathbf{d}}_u^{\mathcal{P}_4})+\tilde{d}_u^{\mathcal{P}_4}}\geq\eta,\forall u,\end{cases} \tag{31}$$

where $\lambda_{\boldsymbol{\phi}}=\frac{f_t(\boldsymbol{\phi},\boldsymbol{\varphi})}{g_t(\boldsymbol{\phi},\boldsymbol{\varphi})}$ denotes the Dinkelbach parameter. Utilizing the first-order Taylor approximation, we simplify problem $\mathcal{P}_{4.2}$ as

$$\mathcal{P}_{4.3}\begin{cases}\underset{\boldsymbol{\phi},\boldsymbol{\varphi}}{\text{minimize}}\ \lambda_{\boldsymbol{\phi}}g_t(\boldsymbol{\phi},\boldsymbol{\varphi})-\hat{f}_t(\boldsymbol{\phi},\boldsymbol{\varphi})\\ \text{subject to } |\boldsymbol{\phi}|=1, |\boldsymbol{\varphi}|=1, \boldsymbol{\phi}-\boldsymbol{\varphi}=\mathbf{0},\\ \qquad\qquad 2\Re(\boldsymbol{\phi}^T\mathbf{p}_u^{\mathcal{P}_4})\leq const.,\forall u.\end{cases} \tag{32}$$

where $\hat{f}_t(\boldsymbol{\phi},\boldsymbol{\varphi})$ is a lower bound function of $f_t(\boldsymbol{\phi},\boldsymbol{\varphi})$ and $\mathbf{p}_u^{\mathcal{P}_4}$ is the reconstructed vector to linearize the SINR constraint. Then, problem $\mathcal{P}_{4.3}$ is solved by the C-ADMM algorithm as the previous work [28].

4. NUMERICAL EXPERIMENTS

In the simulations, RHS, RIS, and MU are equipped with the UPA with $N_x^B\times N_y^B=5\times5$, $N_x^R\times N_y^R=6\times6$, and $N_x^U\times N_y^U=2\times2$ elements, respectively. Meanwhile, BS has $N_{RF}=4$ feeds which are connected with RHS. We deploy a BS at the 3-D position $[0,0,0]$ and a RIS at $[100,100,100]$. A single target is located at $[200,150,50]$, two clutters are at $[300,250,60]$, $[100,125,60]$, respectively, and two user are located at $[400,350,30]$ and $[430,260,30]$. The central frequency of the wideband DFRC is $f_c=10$ GHz and the frequency step of OFDM is set to $\triangle f=20$ MHz. The total number of subcarriers is $K=32$. The inter-element spacing for the RHS, RIS, and MU are set as $\lambda_c/6$, $\lambda_c/2$ and $\lambda_c/2$, respectively. The transmit power at each subcarriers is set to $\mathcal{P}_k=15$ dB, $\forall k$. The noise variances are $\sigma_R^2=-5$dB and $\sigma_C^2=-35$dB. We set the SINR threshold $\eta=10$dB for all users. The maximum iteration for C-ADMM and AM are set as 20 and 30 times.

Fig. 2 shows the achievable radar SINR versus the number of iterations. It is seen that the proposed algorithm converges within around 15 iterations. Obviously, if we optimize the receive filter, digital, holographic and passive beamformer, simultaneously, the highest radar SINR is achieved compared with non-RHS, non-RIS and random RIS. Fig. 3 illustrates the radar SINR versus the communications SINR. In DFRC system, the increase in communications SINR leads to the performance loss for radar SINR. A higher communications SINR exacerbates this loss. Hence, RHS-aided DFRC system requires a performance trade-off between radar and communications.

5. SUMMARY

We considered joint use of the RHS and RIS to assist a wideband DFRC system. Our design of digital, holographic, and passive beamformers shows improvement in the performance of the DFRC system when compared with non-RIS and non-RHS systems. The key challenge to the design problem arises from coupling of various parameters and nonconvexity. We showed that our alternating optimization approach facilitates not only decoupling but also a tractable design.

6. REFERENCES

[1] J. A. Hodge, K. V. Mishra, and A. I. Zaghloul, "Intelligent time-varying metasurface transceiver for index modulation in 6G wireless networks," *IEEE Antennas and Wireless Propagation Letters*, vol. 19, no. 11, pp. 1891–1895, 2020.

[2] Z. Esmaeilbeig, K. V. Mishra, and M. Soltanalian, "IRS-aided radar: Enhanced target parameter estimation via intelligent

reflecting surfaces," in *IEEE Sensor Array and Multichannel Signal Processing Workshop*, 2022, pp. 286–290.

[3] Z. Esmaeilbeig, K. V. Mishra, A. Eamaz, and M. Soltanalian, "Cramér-Rao lower bound optimization for hidden moving target sensing via multi-IRS-aided radar," *arXiv preprint arXiv:2210.05812*, 2022.

[4] M. Di Renzo, A. Zappone, M. Debbah, M.-S. Alouini, C. Yuen, J. de Rosny, and S. Tretyakov, "Smart radio environments empowered by reconfigurable intelligent surfaces: How it works, state of research, and the road ahead," *IEEE Journal on Selected Areas in Communications*, vol. 38, no. 11, pp. 2450–2525, 2020.

[5] Q. Wu and R. Zhang, "Intelligent reflecting surface enhanced wireless network via joint active and passive beamforming," *IEEE Transactions on Wireless Communications*, vol. 18, no. 11, pp. 5394–5409, 2019.

[6] S. Buzzi, E. Grossi, M. Lops, and L. Venturino, "Foundations of MIMO radar detection aided by reconfigurable intelligent surfaces," *IEEE Transactions on Signal Processing*, vol. 70, pp. 1749–1763, 2022.

[7] W. Tang, M. Z. Chen, X. Chen, J. Y. Dai, Y. Han, M. Di Renzo, Y. Zeng, S. Jin, Q. Cheng, and T. J. Cui, "Wireless communications with reconfigurable intelligent surface: Path loss modeling and experimental measurement," *IEEE Transactions on Wireless Communications*, vol. 20, no. 1, pp. 421–439, 2021.

[8] K. V. Mishra, A. Chattopadhyay, S. S. Acharjee, and A. P. Petropulu, "OptM3Sec: Optimizing multicast IRS-aided multi-antenna DFRC secrecy channel with multiple eavesdroppers," in *IEEE International Conference on Acoustics, Speech and Signal Processing*, 2022, pp. 9037–9041.

[9] A. M. Elbir, K. V. Mishra, M. Shankar, and S. Chatzinotas, "The rise of intelligent reflecting surfaces in integrated sensing and communications paradigms," *arXiv preprint arXiv:2204.07265*, 2022.

[10] T. Wei, L. Wu, K. V. Mishra, and M. R. B. Shankar, "Multi-IRS-aided Doppler-tolerant wideband DFRC system," *arXiv preprint arXiv:2207.02157*, 2022.

[11] K. V. Mishra, M. B. Shankar, V. Koivunen, B. Ottersten, and S. A. Vorobyov, "Toward millimeter-wave joint radar communications: A signal processing perspective," *IEEE Signal Processing Magazine*, vol. 36, no. 5, pp. 100–114, 2019.

[12] R.-B. R. Hwang, "Binary meta-hologram for a reconfigurable holographic metamaterial antenna," *Scientific Reports*, vol. 10, no. 1, pp. 1–10, 2020.

[13] R. Deng, B. Di, H. Zhang, D. Niyato, Z. Han, H. V. Poor, and L. Song, "Reconfigurable holographic surfaces for future wireless communications," *IEEE Wireless Communications*, vol. 28, no. 6, pp. 126–131, 2021.

[14] R. Deng, B. Di, H. Zhang, Y. Tan, and L. Song, "Reconfigurable holographic surface-enabled multi-user wireless communications: Amplitude-controlled holographic beamforming," *IEEE Transactions on Wireless Communications*, vol. 21, no. 8, pp. 6003–6017, 2022.

[15] B. Di, "Reconfigurable holographic metasurface aided wideband OFDM communications against beam squint," *IEEE Transactions on Vehicular Technology*, vol. 70, no. 5, pp. 5099–5103, 2021.

[16] S. Zeng, H. Zhang, B. Di, H. Qin, X. Su, and L. Song, "Reconfigurable refractive surfaces: An energy-efficient way to holographic MIMO," *IEEE Communications Letters*, pp. 1–1, 2022.

[17] H. Zhang, H. Zhang, B. Di, M. D. Renzo, Z. Han, H. V. Poor, and L. Song, "Holographic integrated sensing and communication," *IEEE Journal on Selected Areas in Communications*, vol. 40, no. 7, pp. 2114–2130, 2022.

[18] D. Dardari and N. Decarli, "Holographic communication using intelligent surfaces," *IEEE Communications Magazine*, vol. 59, no. 6, pp. 35–41, 2021.

[19] Z. Wan, Z. Gao, F. Gao, M. D. Renzo, and M.-S. Alouini, "Terahertz massive MIMO with holographic reconfigurable intelligent surfaces," *IEEE Transactions on Communications*, vol. 69, no. 7, pp. 4732–4750, 2021.

[20] A. M. Elbir, K. V. Mishra, and S. Chatzinotas, "Terahertz-band joint ultra-massive MIMO radar-communications: Model-based and model-free hybrid beamforming," *IEEE Journal of Special Topics in Signal Processing*, vol. 15, no. 6, pp. 1468–1483, 2021.

[21] H. Li, W. Cai, Y. Liu, M. Li, Q. Liu, and Q. Wu, "Intelligent reflecting surface enhanced wideband MIMO-OFDM communications: From practical model to reflection optimization," *IEEE Transactions on Communications*, vol. 69, no. 7, pp. 4807–4820, 2021.

[22] M. Wang, F. Gao, S. Jin, and H. Lin, "An overview of enhanced massive MIMO with array signal processing techniques," *IEEE Journal of Selected Topics in Signal Processing*, vol. 13, no. 5, pp. 886–901, 2019.

[23] E. Vlachos, G. C. Alexandropoulos, and J. Thompson, "Wideband MIMO channel estimation for hybrid beamforming millimeter wave systems via random spatial sampling," *IEEE Journal of Selected Topics in Signal Processing*, vol. 13, no. 5, pp. 1136–1150, 2019.

[24] E. Shtaiwi, H. Zhang, S. Vishwanath, M. Youssef, A. Abdelhadi, and Z. Han, "Channel estimation approach for RIS assisted MIMO systems," *IEEE Transactions on Cognitive Communications and Networking*, vol. 7, no. 2, pp. 452–465, 2021.

[25] A. Aubry, A. De Maio, and M. M. Naghsh, "Optimizing radar waveform and Doppler filter bank via generalized fractional programming," *IEEE Journal of Selected Topics in Signal Processing*, vol. 9, no. 8, pp. 1387–1399, 2015.

[26] T. Wei, L. Wu, K. V. Mishra, and M. R. B. Shankar, "Multiple IRS-assisted wideband dual-function radar-communication," in *IEEE International Symposium on Joint Communications & Sensing*, 2022, pp. 1–5.

[27] K. Alhujaili, V. Monga, and M. Rangaswamy, "Transmit MIMO radar beampattern design via optimization on the complex circle manifold," *IEEE Transactions on Signal Processing*, vol. 67, no. 13, pp. 3561–3575, 2019.

[28] J. Yang, G. Cui, X. Yu, and L. Kong, "Dual-use signal design for radar and communication via ambiguity function sidelobe control," *IEEE Transactions on Vehicular Technology*, vol. 69, no. 9, pp. 9781–9794, 2020.